IMA Journal of Applied Mathematics (2019) **84**, 1022–1043
doi:10.1093/imamat/hxz024
Advance Access publication on 7 October 2019

Maximal 3D printing extrusion rates

D. A. Edwards*
Department of Mathematical Sciences, University of Delaware, Newark, DE 19716, USA
*Corresponding author: dedwards@udel.edu

M. E. Mackay, Z. R. Swain and C. R. Banbury
Department of Materials Science and Engineering, University of Delaware, Newark, DE 19716, USA

and

D. D. Phan
Department of Chemical and Biomolecular Engineering, University of Delaware, Newark, DE 19716, USA

[Received on 25 January 2019; revised on 22 July 2019; accepted on 27 August 2019]

Many applications of 3D printing are enhanced by increased printing speed. In the hot end of a 3D printer, the polymer feed stock flows in a heated cylinder at a set temperature. Since the polymer must be hot enough to reach a pliant state before extrusion, this establishes a maximum velocity beyond which the polymer is too rigid to be extruded. A mathematical model is presented for this system, and both amorphous and crystalline polymer systems are examined. The former is a heat transfer problem; the latter is a Stefan problem. Several different conditions for establishing the maximum velocity are considered; using the average polymer temperature in the hot end matches well with experimental data.

Keywords: 3D printing; additive manufacturing; extrusion rates; heat transfer; asymptotics; Stefan problem.

1. Introduction

In recent years, 3D printing (or additive manufacturing) has become popular for various types of production, from industrial production of prototypes to consumer production of various devices and gadgets (Gibson *et al.*, 2009). In many situations, it is desirable to manufacture the products as quickly as possible. However, due to the design of the printing head, there is a natural upper bound to the velocity.

In a 3D printer, a rigid polymer fiber is inserted at some pressure into a 'hot end', which we consider to be a cylinder of radius $R_{\max}$ (see Fig. 1). Within the hot end, the polymer is heated so that it becomes pliant, and then is extruded through a nozzle of smaller radius. Engineers would like to extrude the polymer as quickly as possible to reduce processing times. However, increasing the velocity of the extrusion reduces the heating time, eventually leading to a case where the polymer is rigid enough that the pressure needed to extrude it is greater than that exerted by the insertion pump. Therefore, given a temperature differential in the hot end (which is fixed by device specifications), we wish to find the maximum feed velocity that will guarantee extrusion.

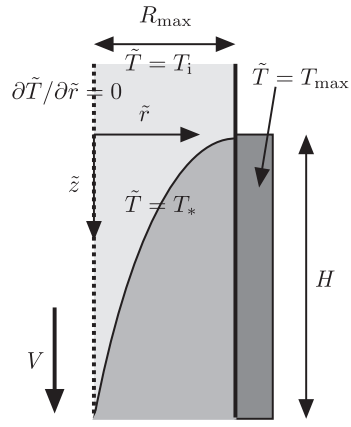

FIG. 1. Cross-section of half of hot end, dimensional coordinates. Light area is rigid polymer, medium area is pliant polymer, dark area is heater. The extrusion nozzle is downstream.

We model the system as a heat transfer problem in cylindrical coordinates in Section 2. There are two main types of polymers used in 3D printing: amorphous and crystalline. In the amorphous case treated in Section 3, the rigid and pliant regions have similar material properties, and the problem has an analytically tractable solution. However, it is not obvious which constraint on the mathematical system translates into a velocity bound that matches the experimental data. We consider three possibilities: the minimum exit temperature, the average temperature in the hot end and a condition on the polymer viscosity.

As shown in Section 4, a formal treatment of the crystalline case involves a Stefan-like problem. Introducing the quasistationary approximation yields analytically tractable solutions. In Section 5, the same possible mathematical constraints are used to compare the solution with experimental data. In Section 6 we use results from the amorphous model to compare to crystalline polymer data.

Our results demonstrate that using the average temperature as a mathematical condition for the amorphous model produces an estimate for the velocity upper bound, which matches well with experimental data, no matter the type of polymer used.

2. Governing equations

We model the system as shown in Fig. 1. We consider heat transfer of an initially rigid polymer passing through a cylinder, and then becoming pliant under heating. If the polymer is crystalline, we define 'pliant' to mean 'melted'. If the polymer is amorphous, we define 'pliant' as having undergone the glass–rubber phase transition.

Complete models for the entire system may be quite complex, necessitating numerical approaches (Lotero *et al.*, 2017; Mu *et al.*, 2015; Sandoval Murillo *et al.*, 2017; Schoinochoritis *et al.*, 2017). However, our goal is quite different: to calculate an upper bound on the extrusion velocity, and relate it directly to other parameters in the problem. Therefore, a much simpler model (once which allows analytical solutions) is desirable. Happily, it will be shown that such a reduced model provides accurate results.

Therefore, in the system at hand, we make the following simplifications:

1. The problem is radially symmetric, so diffusion in the angular direction may be neglected.

2. The aspect ratio of the heater is small, so diffusion in the vertical direction may be neglected.
3. The velocity is a constant V in the $\tilde{z}$-direction (see Fig. 1). This is a realistic assumption at the inserted end because the fiber is slightly smaller than the tube, and hence will slide easily inside it. Once the polymer becomes more pliant and liquid-like, it will develop into Poiseuille or more complicated non-Newtonian flow. We ignore those details for now, and just consider V to be the average of the velocity profile.
4. We are interested in the stationary problem; i.e. the steady-state flow after all transients have decayed away.
5. We ignore the narrowing of the hot end to the small nozzle at the extrusion point. In particular, we will solve in the portion of the hot end before it narrows, and use facts about the temperature there to determine whether the polymer will extrude.

With these assumptions, the general dimensional equation is given by

$$\rho c_p V \frac{\partial \tilde{T}}{\partial \tilde{z}} = \frac{k}{\tilde{r}} \frac{\partial}{\partial \tilde{r}} \left(\tilde{r} \frac{\partial \tilde{T}}{\partial \tilde{r}} \right), \qquad 0 \leq \tilde{r} \leq R_{\max}, \tag{2.1}$$

where $\tilde{T}$ is the temperature of the polymer, ρ the density, c_p the heat capacity and k the thermal conductivity.

We assume that the heater is of length H; we denote $\tilde{z} = 0$ to be its upper end. The heater maintains the surface $\tilde{r} = R_{\max}$ at a fixed temperature $\tilde{T} = T_{\max} > T_*$, where T_* is the pliancy temperature. (Depending on the polymer, it may be considered the glass–rubber transition temperature or the melting temperature.) The rigid polymer is inserted at $\tilde{z} = 0$ at an 'insertion temperature' $T_{\mathrm{i}} < T_*$.

Motivated by these conditions, we introduce the following scalings:

$$r = \frac{\tilde{r}}{R_{\max}}, \qquad z = \frac{\tilde{z}}{H}, \qquad T(r,z) = \frac{\tilde{T}(\tilde{r},\tilde{z}) - T_*}{\Delta T}, \qquad \Delta T = T_* - T_{\mathrm{i}}. \tag{2.2}$$

Substituting (2.2) into (2.1), we have the following:

$$\frac{\partial T}{\partial z} = \mathrm{Pe}^{-1} \frac{1}{r} \frac{\partial}{\partial r} \left(r \frac{\partial T}{\partial r} \right), \qquad \mathrm{Pe} = \frac{\rho c_p R_{\max}^2 V}{kH}. \tag{2.3}$$

Obviously if the Péclet number $\mathrm{Pe} \ll 1$, then the right-hand side dominates. In that case, there is time for heat to diffuse through the polymer and make it completely pliant before it is extruded. The question is as follows: how large can V be and still guarantee that process?

In dimensionless coordinates, the boundary and initial conditions described above become

$$T_{\mathrm{p}}(1,z) = \alpha, \qquad \alpha = \frac{T_{\max} - T_*}{\Delta T} > 0, \tag{2.4a}$$

$$T_{\mathrm{r}}(r,0) = -1. \tag{2.4b}$$

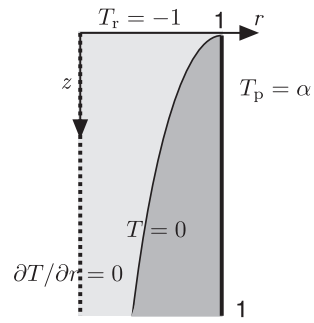

FIG. 2. Idealized dimensionless system. Note we consider only up to $z = 1$.

Since $T_{max} > T_*$, the polymer will always be pliant at the exposed surface; hence, we use the subscript 'p'. Similarly, since $T_i < T_*$, the polymer will always be rigid initially; hence, we use the subscript 'r'. The last boundary condition required is that the centerline of the cylinder has no flux through it:

$$\frac{\partial T}{\partial r}(0, z) = 0. \tag{2.5}$$

Given assumption 2 of no z-diffusion, we cannot impose exit conditions on the heater. Hence, we simply solve the problem for all z, and then just examine the solution for $z \in [0, 1]$ (see Fig. 2). In other words, we determine the behavior of the polymer while heated, and infer from that what conditions are needed to make sure it is pliant enough to be extruded through the downstream nozzle.

We will discuss the final condition (how to establish the temperature bound) in the next section.

3. The amorphous case

3.1 *Solution*

We begin with a discussion of the amorphous case, which is simpler. In these polymers, there is no melting, just a glass–rubber phase transition. Therefore, the pliancy temperature T_* is just the glass–rubber transition temperature T_g. Moreover, we assume that the material parameters do not change drastically as the polymer undergoes the glass–rubber transition, and hence we do not have to track a moving boundary between the phases. Thus, in this section we drop all subscripts on the dependent variable T.

The problem then reduces to solving (2.3) subject to (2.4) and (2.5). We may set up a problem with homogeneous boundary conditions by letting

$$T(r, z) = \alpha - (\alpha + 1)\Theta(r, z). \tag{3.1a}$$

With this substitution, it is a standard but tedious exercise in separation of variables to show that

$$\Theta(r, z) = \sum_{n=1}^{\infty} \frac{2}{j_{0,n} J_1(j_{0,n})} \exp\left(-\frac{j_{0,n}^2 z}{\mathrm{Pe}}\right) J_0(j_{0,n} r), \tag{3.1b}$$

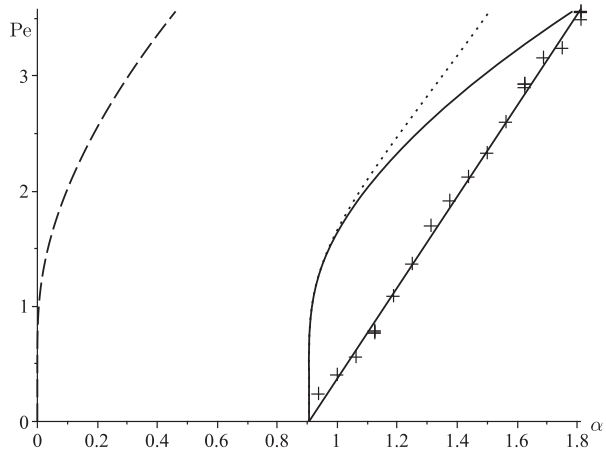

FIG. 3. Graph of solution using exit conditions. Dashed curve: (3.3) (five terms). Solid curve: (3.5) (five terms). Dotted curve: (3.6b). Crosses: experimental data for acrylonitrile butadiene styrene (ABS) from Mackay *et al.* (2017) (with linear fit). Note that neither theoretical curve matches the behavior of the data.

where $j_{0,n}$ is the nth zero of J_0, the zeroth Bessel function of the first kind.

The problem may also be written as a series using Laplace transform techniques, as in Carrier & Pearson (1988), (Section 2.3). However, such series are typically good for large z, which is not the region in which we are interested.

3.2 *Exit temperature as threshold condition*

Given this solution, we must specify a condition that corresponds to a state that allows extrusion of the polymer. As a first possibility, we simply check if the polymer is pliant at the exit of the hot end ($z = 1$). Experimental evidence suggests that if the polymer is rigid in any part of the domain, it will clog the nozzle. Since the polymer is coldest at the center, we must require that

$$T(0, 1) \geq 0, \tag{3.2}$$

with the borderline case being equality.

Substituting (3.1) into the equality form of (3.2), we have

$$\alpha = \frac{\Theta(0,1)}{1 - \Theta(0,1)}, \qquad \Theta(0,1) = \sum_{n=1}^{\infty} \frac{2}{j_{0,n} J_1(j_{0,n})} \exp\left(-\frac{j_{0,n}^2}{\mathrm{Pe}}\right). \tag{3.3}$$

(The $j_{0,n}$ increase quickly with n, so we normally need to take only a few terms in the sum.)

A plot of (3.3) is shown as the dashed curve in Fig. 3, which uses the parameters in Tables A1 and A2 in the Appendix. Here the curves are presented in the α-Pe plane. Recall that α is a scaled version of $T_{\max}$, and Pe is a scaled version of V, so this choice provides the experimentalist with the maximum velocity for a given temperature differential.

Note that the dashed curve does not match the experimental data, which has a Pe-intercept greater than zero. This corresponds to a non-zero T value for which extrusion stops. Therefore, we replace

(3.2) with

$$T(0,1) \geq T_{\mathrm{t}}, \tag{3.4}$$

for some threshold temperature $0 < T_{\mathrm{t}} < \alpha$, which can be inferred from experiments. This makes physical sense, since after leaving the heated region, the polymer will cool as it is forced through the unheated nozzle. Hence, the polymer must be hotter than T_* (α in the dimensionless context) in order to remain pliant at the end of the nozzle. In addition, by adopting the form (3.4), we can essentially ignore complications associated with device geometry, etc., since those are then incorporated into the threshold T_{t}, which is determined from the data.

Replicating our previous analysis, we have the following:

$$\alpha = \frac{\Theta(0,1) + T_{\mathrm{t}}}{1 - \Theta(0,1)}, \tag{3.5}$$

where $\Theta(0,1)$ is given by (3.3). A plot of this solution is shown as the solid curve in Fig. 3. In this case, the Pe-intercepts match, since we fit T_{t} to the data. However, the behavior of the curve itself is again far from the data, especially for low Pe. In this limit, the first term in the sum in (3.3) dominates, so we have

$$\Theta(0,1) \sim \frac{2}{j_{0,1} J_1(j_{0,1})} \exp\left(-\frac{j_{0,1}^2}{\mathrm{Pe}}\right), \tag{3.6a}$$

which is also small, so we can expand the right-hand side of (3.5) to obtain

$$\alpha \sim T_{\mathrm{t}} + \frac{2(1+T_{\mathrm{t}})}{j_{0,1} J_1(j_{0,1})} \exp\left(-\frac{j_{0,1}^2}{\mathrm{Pe}}\right). \tag{3.6b}$$

Therefore, the graph approaches $(\alpha, 0)$ exponentially from above, as shown. This is illustrated as the dotted curve in Fig. 3. If we compare the slope of the dotted curve for large Pe to the best-fit line through the data, we see that they are similar (though the slope of the dotted curve is slightly larger). However, the curve has shifted from the data.

3.3 *Viscosity as threshold condition*

The poor agreement in Fig. 3 motivates a reconsideration of the threshold condition. In particular, we recall that the process stops when the insertion pump pressure is less than that needed to extrude the polymer. The pressure depends on the viscosity μ, which we assume to follow the temperature-dependent model (Bird *et al.*, 1960, Section 1.5)

$$\mu(r,z) = \exp\left(\frac{\tilde{T}_\mu}{\tilde{T}(r,z)}\right) = \exp\left(\frac{\tilde{T}_\mu}{T_* + (\Delta T)T}\right), \tag{3.7}$$

where $\tilde{T}_\mu$ is some constant. In this case, (3.2) and (3.4) can be seen as specifying a particular viscosity at the exit that corresponds to $T = T_{\mathrm{t}}$.

For now, we treat the polymer as a Newtonian fluid. (The model will become irrelevant, as we see below.) If we assume that the flow is unidirectional, then the momentum balance becomes

$$\frac{\mathrm{d}p}{\mathrm{d}z} = \frac{1}{r}\frac{\partial}{\partial r}\left(\mu(r,z)r\frac{\partial v_z}{\partial r}\right), \tag{3.8}$$

where $p(z)$ is the pressure. (Note that all quantities are considered dimensionless—the exact normalization factors are irrelevant, as described in more detail below.) But (3.8) cannot be satisfied, since the right-hand side depends explicitly on r in a non-parametric fashion.

Hence, in general we would not expect unidirectional flow. This makes sense, since the flow near the heated surface would have a lower viscosity and would hence flow faster than the core, which would force a radial flow to the heated surface. However, we expect these deviations to be small, so we approximate μ by its cross-sectional average:

$$\mu(r,z) \approx \langle\mu\rangle(z) = 2\int_0^1 r\mu(r,z)\,\mathrm{d}r. \tag{3.9}$$

Substituting this expression into (3.8), we have

$$\frac{\mathrm{d}p}{\mathrm{d}z} = \langle\mu\rangle(z)\left[\frac{1}{r}\frac{\mathrm{d}}{\mathrm{d}r}\left(r\frac{\mathrm{d}v_z}{\mathrm{d}r}\right)\right]. \tag{3.10}$$

Equation (3.10) now satisfies the assumptions of unidirectional flow, since the bracketed quantity must be constant, which leads to the normal parabolic Poiseuille flow.

Thus, the pressure head needed to extrude the polymer is given by integrating (3.10):

$$\int_0^1 \frac{\mathrm{d}p}{\mathrm{d}z} \propto \int_0^1 \langle\mu\rangle(z)\,\mathrm{d}z$$

$$p(1) \propto \bar{\mu}, \qquad \bar{\mu} = 2\int_0^1\int_0^1 r\mu(r,z)\,\mathrm{d}r\,\mathrm{d}z. \tag{3.11}$$

Here we have used gauge pressure and absorbed the constant bracketed quantity in (3.10) into the proportionality symbol. That is because the exact factors are irrelevant. The key insight from (3.11) is that the pressure head is not related to the viscosity (and hence the temperature) at the exit; it is related to the average viscosity.

In particular, we note from our previous discussion that if $\mathrm{Pe} \to 0$, then $\Theta \to 0$, and $\alpha \to T_\mathrm{t}$. As $\mathrm{Pe} \to 0$, the polymer flows very slowly, so by the time it reaches $z = 1$, its temperature will equilibrate to α. Hence for extrusion to occur, $T_\mathrm{t} = \alpha$ in this case. Therefore, we see from (3.7) that the threshold for the viscosity would be

$$\mu_\mathrm{t} = \exp\left(\frac{\tilde{T}_\mu}{T_* + (\Delta T)T_\mathrm{t}}\right). \tag{3.12}$$

Given the form (3.7), calculating $\bar{\mu}$ using (3.11) is quite difficult. However, we may obtain results by exploiting the averaging idea. In particular, we wish to preserve the assumption that μ is a function

only of z. So we define

$$\mu(z) = \exp\left(\frac{\tilde{T}_\mu}{T_* + (\Delta T)\langle T\rangle}\right), \tag{3.13}$$

where $\langle T\rangle$ is defined as in (3.9). (Note that we do not denote the quantity in (3.13) as $\langle\mu\rangle$, because we construct it by averaging the temperature, not μ.) Then at extrusion, the averaged viscosity $\bar{\mu}$ must equal μ_t, so we have

$$\mu_\mathrm{t} = \int_0^1 \exp\left(\frac{\tilde{T}_\mu}{T_* + (\Delta T)\langle T\rangle}\right) \mathrm{d}z \tag{3.14a}$$

$$= \int_0^1 \exp\left(\frac{\tilde{T}_\mu}{T_* + (\Delta T)[\alpha - (\alpha+1)\langle\Theta\rangle]}\right) \mathrm{d}z, \tag{3.14b}$$

where we have used (3.1a).

Motivated by previous work, we take the limit of small Pe, which corresponds to small Θ. Also, we know that in this case, $\alpha \to T_\mathrm{t}$. Therefore, motivated by (3.6b), we let

$$\alpha = T_\mathrm{t} + (T_\mathrm{t}+1)\alpha_1, \qquad \alpha_1 \ll 1. \tag{3.15}$$

(We expect that $\alpha_1 = O(\mathrm{Pe})$, but we will establish that in the analysis below.) Substituting these assumptions into (3.14b) and expanding using the binomial theorem, we obtain

$$\mu_\mathrm{t} \sim \int_0^1 \exp\left(\frac{\tilde{T}_\mu}{T_* + T_\mathrm{t}\Delta T}\left(1 - \frac{\Delta T(T_\mathrm{t}+1)(\alpha_1 - \langle\Theta\rangle)}{T_* + T_\mathrm{t}\Delta T}\right)\right) \mathrm{d}z,$$

which can be simplified into the following expression:

$$e^{\beta\alpha_1} = \int_0^1 e^{\beta\langle\Theta\rangle}\,\mathrm{d}z, \qquad \beta = \frac{\tilde{T}_\mu(\Delta T)(T_\mathrm{t}+1)}{(T_* + T_\mathrm{t}\Delta T)^2}. \tag{3.16}$$

To approximate the integral, we exploit the fact that the terms in (3.1b) decay quickly with increasing n for small Pe. (This is true even in the case that $z \to 0$, but then the decay isn't exponential.) Therefore, we replace the sum (3.1b) with its first term in the integral above to yield

$$e^{\beta\alpha_1} = \frac{\mathrm{Pe}}{j_{0,1}^2}\left[\mathrm{Ei}\left(\frac{4\beta}{j_{0,1}^2}\right) - \mathrm{Ei}\left(\frac{4\beta}{j_{0,1}^2}\exp\left(-\frac{j_{0,1}^2}{\mathrm{Pe}}\right)\right)\right],$$

where Ei is the exponential integral, defined as

$$\mathrm{Ei}(y) = \int_{-\infty}^{y} \frac{e^{y'}}{y'}\,\mathrm{d}y'.$$

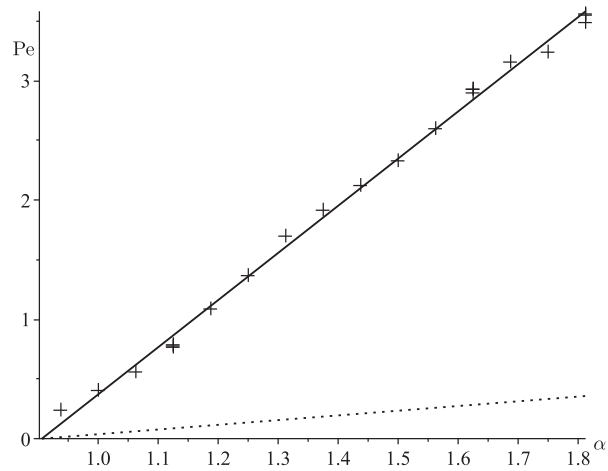

FIG. 4. ABS data fitting using (3.18). Dotted line: $\beta = 8.16$ given in Table A2. Solid line: data with best fit ($\beta = 0.58$).

Then expanding for small Pe, we have the following:

$$e^{\beta\alpha_1} = 1 + \frac{\mathrm{Pe}}{j_{0,1}^2}\left[\mathrm{Ei}\left(\frac{4\beta}{j_{0,1}^2}\right) - \log\left(\frac{4\beta}{j_{0,1}^2}\right) - \gamma\right], \tag{3.17}$$

where γ is Euler's constant. Since the right-hand side is very close to 1, that establishes that $\alpha_1 = O(\mathrm{Pe})$. Expanding the left-hand side for small α_1 and then substituting the result into (3.15) and rearranging, we have

$$\alpha = T_\mathrm{t} + (T_\mathrm{t} + 1)\frac{\mathrm{Pe}}{j_{0,1}^2\beta}\left[\mathrm{Ei}\left(\frac{4\beta}{j_{0,1}^2}\right) - \log\left(\frac{4\beta}{j_{0,1}^2}\right) - \gamma\right]. \tag{3.18}$$

A plot of (3.18) is shown as the dotted line in Fig. 4. Given the poor fit, it is clear that this condition is not appropriate for determining the maximum extrusion velocity.

To determine the problem, we re-examine (3.13) in light of our results. Not only does μ depend exponentially on T, but the argument of the exponent will be very large due to the size of $\tilde{T}_\mu$ (see the Appendix). Hence, even small errors will have a large effect. For instance, with reasonable parameter values, even a 1% error in $\langle T\rangle$ can cause a 25% error in μ. Thus, though our various averaging approximations may simplify the analysis, they introduce small errors, which magnify in the exponential.

3.4 *Average temperature as threshold condition*

Nevertheless, the averaging idea remains intuitive. The failure mode for the device is pressure buildup, which is driven by the material properties throughout the hot end, not just at one point or cross section. Therefore, we retain the averaging idea, but in a simpler context. Instead of using the average viscosity, as a substitute we simply require that the average temperature be above T_t:

$$\bar{T} \geq T_\mathrm{t}, \tag{3.19}$$

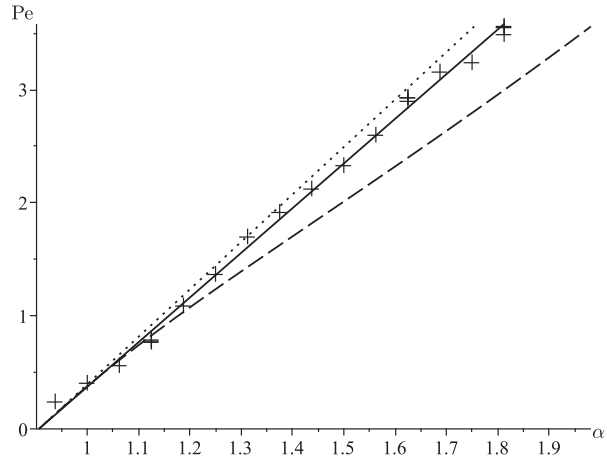

FIG. 5. Graph of solution using averaged conditions. Dashed curve: (3.20) (five terms). Dotted curve: (3.22). Crosses: ABS experimental data (with linear fit). Note the reasonably good agreement.

where the bar notation is defined as in (3.11).

Substituting (3.1) into (3.19) and rearranging, we obtain

$$\alpha = \frac{\bar{\Theta} + T_{\mathrm{t}}}{1 - \bar{\Theta}}, \qquad \bar{\Theta} = \sum_{n=1}^{\infty} \frac{4\,\mathrm{Pe}}{j_{0,n}^4} \left[1 - \exp\left(-\frac{j_{0,n}^2}{\mathrm{Pe}} \right) \right]. \tag{3.20}$$

A plot of (3.20) is shown as the dashed curve in Fig. 5. Here this curve begins to diverge from the linear fit as Pe increases. Motivated by the good agreement between the asymptotic and full solution in Fig. 3, we do the same asymptotic work here for small Pe. In this case, the exponentials are all negligible and we have

$$\alpha \sim T_{\mathrm{t}} + 4\,\mathrm{Pe}(1 + T_{\mathrm{t}}) \sum_{n=1}^{\infty} \frac{1}{j_{0,n}^4}. \tag{3.21}$$

The sum in (3.21) can be found to be 1/32 (Sneddon, 1960, Eq. (41)); hence, the expression can be written in terms of Pe as follows:

$$\mathrm{Pe} \sim \frac{8(\alpha - T_{\mathrm{t}})}{1 + T_{\mathrm{t}}}. \tag{3.22}$$

Equation (3.22) is illustrated as the dotted curve in Fig. 5. Note the agreement is much better.

4. Crystalline case

4.1 *Governing equations*

We next consider the crystalline case, so we interpret T_* as the melting temperature T_{m}. In this case, there is a melting front $r = s(z)$ separating the rigid and pliant regions:

$$T_{\mathrm{r}}(s(z), z) = T_{\mathrm{p}}(s(z), z) = 0, \qquad s(0) = 1. \tag{4.1}$$

Note that T_r holds in the rigid lightly shaded region $0 < r < s$ in Fig. 1, while T_p holds in the pliant medium shaded region $s < r < 1$.

The formulation of the Stefan condition is not straightforward in the laboratory frame. In particular, the typical time-derivative operator in the heat equation has been replaced by the spatial derivative that arises from the convection of the polymer down the cylinder [see (2.1)]. However, by switching to a moving reference frame, one may derive the proper Stefan condition:

$$\left[-k\frac{\partial \tilde{T}}{\partial \tilde{r}}\right]_{\tilde{s}} = \rho c_\mathrm{L} V \frac{\mathrm{d}\tilde{s}}{\mathrm{d}\tilde{z}},$$

where c_L is the latent heat of melting and $[\cdot]_{\tilde{s}}$ means the jump across the front. (Recall that by assumption, the only flux is in the $\tilde{r}$-direction.) Introducing the scalings from Section 2, we obtain

$$\mathrm{St}\left[\mathrm{Pe}^{-1}\frac{\partial T}{\partial r}\right]_s = -\frac{\mathrm{d}s}{\mathrm{d}z}, \qquad \mathrm{St} = \frac{\Delta T c_p}{c_\mathrm{L}}, \tag{4.2}$$

where St is the Stefan number. (Note that the amorphous system is just a special case, since then $c_\mathrm{L} = 0$, $\mathrm{St} = \infty$ and the condition is that the fluxes must match across any boundary.)

The change in boundary conditions makes the full solution of this problem quite difficult. Motivated by Mackay *et al.* (2017), we treat c_p (and hence Pe) as a constant across phases. Summarizing our system with this assumption, in the rigid region, we have

$$\frac{\partial T_\mathrm{r}}{\partial z} = \frac{\mathrm{Pe}^{-1}}{r}\frac{\partial}{\partial r}\left(r\frac{\partial T_\mathrm{r}}{\partial r}\right), \quad 0 < r < s(z); \qquad \frac{\partial T_\mathrm{r}}{\partial r}(0,z) = 0, \quad T_\mathrm{r}(r,0) = -1. \tag{4.3}$$

In the pliant region, we obtain

$$\frac{\partial T_\mathrm{p}}{\partial z} = \frac{\mathrm{Pe}^{-1}}{r}\frac{\partial}{\partial r}\left(r\frac{\partial T_\mathrm{p}}{\partial r}\right), \quad s(z) < r < 1; \qquad T_\mathrm{p}(1,z) = \alpha. \tag{4.4}$$

At the front $r = s(z)$, we have the following conditions:

$$T_\mathrm{r}(s(z),z) = T_\mathrm{p}(s(z),z) = 0, \qquad s(0) = 1, \tag{4.5a}$$

$$\mathrm{Pe}^{-1}\frac{\partial T_\mathrm{p}}{\partial r}(s(z),z) - \mathrm{Pe}^{-1}\frac{\partial T_\mathrm{r}}{\partial r}(s(z),z) = -\frac{1}{\mathrm{St}}\frac{\mathrm{d}s}{\mathrm{d}z}. \tag{4.5b}$$

4.2 *The quasistationary approximation*

The system as posed has no analytic solution, which is the most desirable kind due to the ability to discern parameter dependence easily. To make the problem tractable, we employ the 'quasistationary approximation'. In particular, we neglect the left-hand side of the partial differential equations (PDEs) in (4.3) and (4.4). This is equivalent to taking $\mathrm{Pe} \to 0$, which is equivalent to taking $V \to 0$, so this is the regime in which we are interested. However, by neglecting the evolution term, we will overestimate the speed of $s(z)$ (Alexiades & Solomon, 1992).

When we take the left-hand side of the PDE in (4.3) equal to zero, the resulting operator is a second-order ordinary differential equation (ODE). But there are three boundary conditions to solve in (4.3) and (4.5a). Since we wish to solve the problem for all time, we ignore the initial condition in (4.3) to obtain the following solution in the rigid region:

$$T_{\mathrm{r}} \equiv 0, \qquad r < s(z). \tag{4.6}$$

To satisfy the initial condition, we would have to insert a thin initial layer near $z = 0$. In this region (where the full differential equation in (4.3) would hold), there is rapid diffusion from the initial condition to (4.6). In the previous section, this layer was important in determining the behavior of the data away from $\mathrm{Pe} = 0$, so we may be suspicious that this approximation will perform well. Moreover, this effect will also tend to overestimate the speed of $s(z)$, since it omits the time needed to raise the polymer to the melting temperature.

Taking the left-hand side of the PDE in (4.4) equal to zero and satisfying the conditions in (4.4) and (4.5a), we have

$$T_{\mathrm{p}}(r, z) = \alpha \left(1 - \frac{\log r}{\log s}\right), \qquad s(z) > 0. \tag{4.7}$$

Depending on the experimental conditions, it may be possible for the front to hit the centerline at some $z_1 < 1$:

$$s(z_1) = 0. \tag{4.8}$$

In that case, the steady-state operator must also satisfy the no-flux condition in (4.3), so we have the following:

$$T_{\mathrm{p}}(r, z) = \alpha, \qquad z > z_1. \tag{4.9}$$

To find $s(z)$, we first substitute (4.6) into (4.5b) to yield

$$\mathrm{Pe}^{-1} \frac{\partial T_{\mathrm{p}}}{\partial r}(s(z), z) = -\frac{1}{\mathrm{St}} \frac{\mathrm{d}s}{\mathrm{d}z}.$$

With T_{r} given by (4.6), the problem essentially reduces to a one-phase Stefan problem. Substituting (4.7) into the above, we obtain

$$-\frac{\alpha}{s \log s} = -\frac{\mathrm{Pe}}{\mathrm{St}} \frac{\mathrm{d}s}{\mathrm{d}z}.$$

Note that this equation makes sense only if $\mathrm{St} \neq \infty$; i.e. only in the melting context.

Continuing to simplify, we obtain

$$\frac{\mathrm{d}u}{\mathrm{d}z} = \frac{4\alpha}{\log u} \frac{\mathrm{St}}{\mathrm{Pe}}, \quad u = s^2, \tag{4.10a}$$

$$4\alpha \frac{\mathrm{St}}{\mathrm{Pe}} z - 1 = u(\log u - 1), \tag{4.10b}$$

where in the last line we have used the initial condition in (4.5a) to determine that $u(0) = 1$. The solution for u can be written explicitly in terms of Lambert W-functions, but it is not illuminating.

We note from (4.10b) that the melting front hits the center of the cylinder when

$$4\alpha \frac{\mathrm{St}}{\mathrm{Pe}} z_1 - 1 = 0 \qquad \Longrightarrow \qquad z_1 = \frac{\mathrm{Pe}}{4\,\mathrm{St}\,\alpha}, \tag{4.11}$$

which matches with Alexiades & Solomon (1992, Section 3.2.C(14)) in the case where $\alpha = 1$. Hence, if $\mathrm{Pe} < 4\,\mathrm{St}\,\alpha$, then the entire polymer melts before it exits the heated region of the cylinder. We note that z_1 depends on the quantity $\mathrm{St}\,\alpha$, which is independent of ΔT (and hence T_i). This makes sense since with the one-phase approximation we are effectively assuming that the polymer enters the chamber at temperature T_*.

5. Crystalline case, proper conditions

5.1 *The exit temperature*

We use the same conditions as in Section 3 to determine if they are appropriate for the crystalline case. First we note from (4.6) and (4.9) that

$$T_\mathrm{r}(0,z) = 0, \qquad z < z_1; \qquad T_\mathrm{p}(0,z) = \alpha, \qquad z > z_1. \tag{5.1}$$

If $T_\mathrm{t} > 0$, conditions (3.2) and (3.4) are really the same (since $T_\mathrm{t} < \alpha$), and are equivalent to

$$\alpha \le \frac{\mathrm{Pe}}{4\,\mathrm{St}} \tag{5.2}$$

from (4.11) with $z_1 = 1$. But as this bound is independent of T_t, we can't shift it to fit the data. This invariance is due to the jump condition inherent in (5.1); however, if we replace (3.4) with $T(\delta, 1) \ge T_\mathrm{t}$ for some small parameter δ, (5.2) still holds in the limit that $\delta \to 0$.

Now we attempt to fit (5.2) to our data using the parameters from Table A3 in the Appendix. Given that $T_\mathrm{m} = 155^\circ$ C, we use only that data for which $T_\mathrm{max} = 170^\circ$ C or higher to ensure that melting has taken place. The results are shown in Fig. 6.

To explain the poor fit, note that since the zero set point for temperature is now T_m, T_t can be negative, which corresponds to it lying between the glass transition temperature T_g and T_m. This is exactly what the data shows. As this case is not contemplated by this condition, the fit is poor. (In particular, if $T_\mathrm{t} < 0$, then the one-phase approach says that flow would occur for all values of Pe.)

5.2 *The viscosity*

We next consider the viscosity approach. As a preliminary approach, we average (4.7) and (4.9) to obtain

$$\langle T_\mathrm{p} \rangle = \alpha \left(1 + \frac{1 - s^2}{2 \log s} \right), \qquad s(z) > 0, \tag{5.3a}$$

$$\langle T_\mathrm{p} \rangle = \alpha, \qquad z > z_1. \tag{5.3b}$$

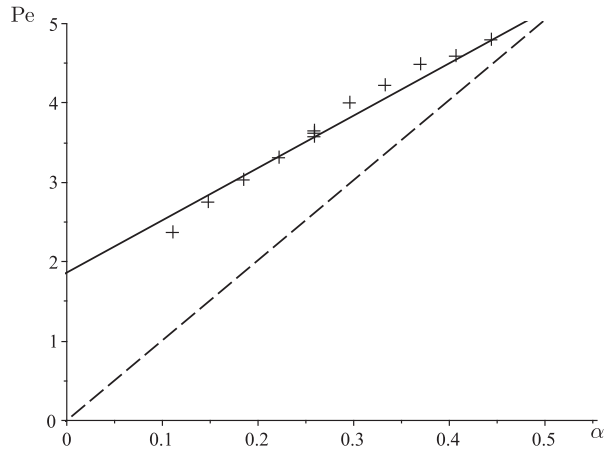

FIG. 6. Graphs of (5.2) (dashed line) with curve fit to polylactic acid (PLA) crystalline data (assumed linear to match models).

Substituting (5.3) into (3.14a) yields

$$\mu_{\mathrm{t}} = \int_1^0 \left(\frac{4\alpha}{\log u}\frac{\mathrm{St}}{\mathrm{Pe}}\right)^{-1} \exp\left(\frac{\tilde{T}_\mu}{T_* + (\Delta T)\alpha[1 + (1-u)/\log u]}\right) \mathrm{d}u + (1 - z_1)\exp\left(\frac{\tilde{T}_\mu}{T_* + (\Delta T)\alpha}\right), \tag{5.4}$$

where we have used (4.5a), (4.8) and (4.10a). Motivated by our previous work, we let

$$\alpha = T_{\mathrm{t}} + \mathrm{Pe}\,\alpha_1, \quad \mathrm{Pe} \to 0. \tag{5.5}$$

Substituting (5.5) into (5.4) and expanding for small Pe using the binomial theorem, we obtain

$$\mu_{\mathrm{t}} = \frac{\mathrm{Pe}\, I}{4\,\mathrm{St}\, T_{\mathrm{t}}} + \mu_t \exp\left(-\frac{\mathrm{Pe}\,\alpha_1(\Delta T)\tilde{T}_\mu}{[T_* + (\Delta T)T_{\mathrm{t}}]^2}\right) - \frac{\mathrm{Pe}}{4\,\mathrm{St}\,\alpha}\mu_t, \tag{5.6a}$$

$$I = -\int_0^1 \log u \exp\left(\frac{\tilde{T}_\mu}{T_* + (\Delta T)T_{\mathrm{t}}[1 + (1-u)/\log u]}\right) \mathrm{d}u, \tag{5.6b}$$

where we have used (4.11). Note also that $I > 0$. Solving (5.6a) for α_1 using (3.16), we have

$$\alpha_1 = \frac{(T_t + 1)a}{4\,\mathrm{St}\, T_{\mathrm{t}}}, \qquad a = \frac{I - \mu_t}{\beta\mu_t}. \tag{5.7}$$

Here we have introduced the variable a to group all the parameters that depend on $\tilde{T}_\mu$. Note that in order for $\alpha_1 > 0$ as required, a must be negative (since $T_{\mathrm{t}} < 0$).

A graph of the comparison is shown in Fig. 7. As previously, it is wildly inaccurate, in part due to the fact that in the experiments chosen, Pe is not small.

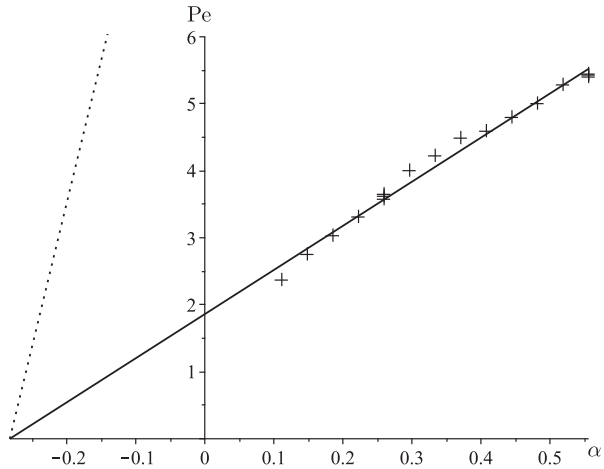

FIG. 7. Graphs of (5.7) (dotted line) with curve fit to PLA crystalline data.

5.3 *The average temperature*

Hence, we conclude with a discussion of the average temperature. Calculating $\bar{T}$ from (5.3), we obtain

$$\bar{T} = \int_0^{z_1} \alpha \left(1 + \frac{1 - s^2}{2 \log s}\right) \mathrm{d}z + \int_{z_1}^1 \alpha \, \mathrm{d}z = \alpha - \frac{\mathrm{Pe}}{8\,\mathrm{St}}. \tag{5.8}$$

Then imposing (3.19), we have

$$\alpha = T_\mathrm{t} + \frac{\mathrm{Pe}}{8\,\mathrm{St}}. \tag{5.9}$$

A comparison with the curve fit is shown in Fig. 8. Even with the shift between (5.2) and (5.9), the fit does not improve. As discussed in Section 5, the quasistationary approximation overestimates the speed of $s(z)$. Hence, for a given V the model overestimates the amount of polymer that is pliant, which would then cause an overestimate of the bound in Pe, as shown in Fig. 8.

6. Using the amorphous model for crystalline polymers

Though PLA can behave in a crystalline manner, the quasisteady approximation outlined in Sections 4 and 5 does not fit the data. The experimental data has $T_\mathrm{t} < T_\mathrm{m}$, which indicates that in some circumstances, the polymer is pliable enough without melting. Therefore, we attempt to match the experimental results by using the amorphous model for PLA.

We replicate the analysis from Section 3.2 and present the results in Fig. 9. Note that in this case we use all the experimental data for PLA, not just those above the melting point. A plot of (3.3) for the PLA data in Tables A3 and A4 is shown as the dashed curve. Note that its behavior does not match the experimental data, which has a Pe-intercept greater than zero. Therefore, we plot (3.5) as the solid curve in Fig. 9. In this case, the Pe-intercepts match, since we fit T_t to the data. Lastly, we use (3.6b), which is illustrated as the dotted curve in Fig. 9. Note that the slope for large Pe is nearly correct.

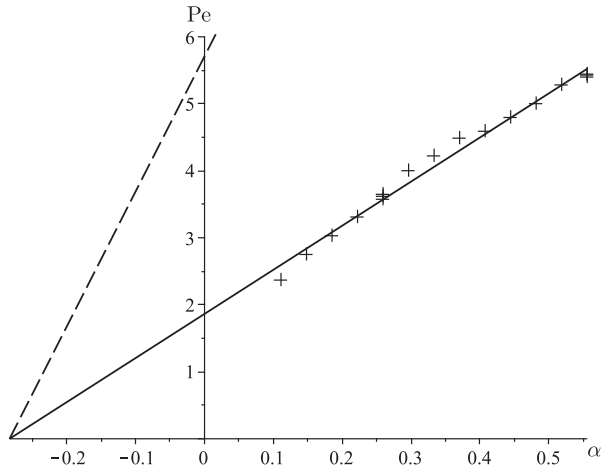

FIG. 8. Graphs of (5.9) (dashed line) with curve fit to PLA crystalline data.

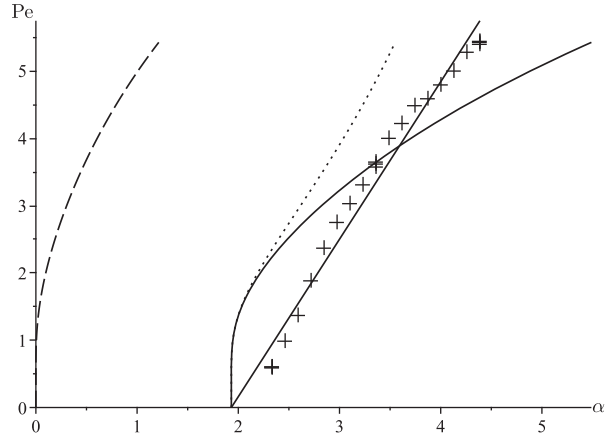

FIG. 9. Graph of solution using exit conditions. Dashed curve: (3.3) (five terms). Solid curve: (3.5) (five terms). Dotted curve: (3.6b). Crosses: PLA experimental data (with linear fit). Note that neither theoretical curve matches the behavior of the data.

Next we use the viscosity model and plot the equivalent of Fig. 4, which is given in Fig. 10. Again, the fit is poor. Moreover, in contrast to Fig. 4, there does not exist a value of β that will actually fit the data.

Because of the poor agreement in both of the above figures, we again use the average temperature as a condition. A plot of (3.20) is shown as the dashed curve in Fig. 11. Though this plot curves somewhat, it does not curve as much as the data. Motivated by the good agreement between the asymptotic and full solution in Fig. 9, we do the same asymptotic work here for small Pe; the expression (3.22) is illustrated as the dotted curve in Fig. 11. Here the agreement is not as strong as in the ABS case, mainly due to the curved nature of the data. However, in the cases of higher temperatures (where we expect the PLA to have melted), the experimental upper bound is sandwiched between the two curves.

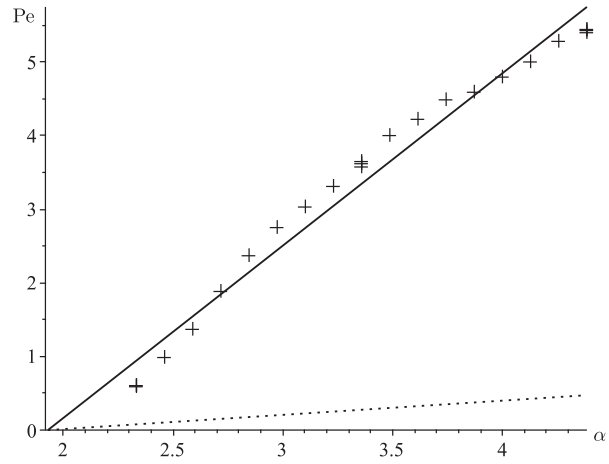

FIG. 10. Data fitting using (3.18). Dotted line: $\beta = 8.81$ as given in Table A4. Solid line: PLA data with linear fit.

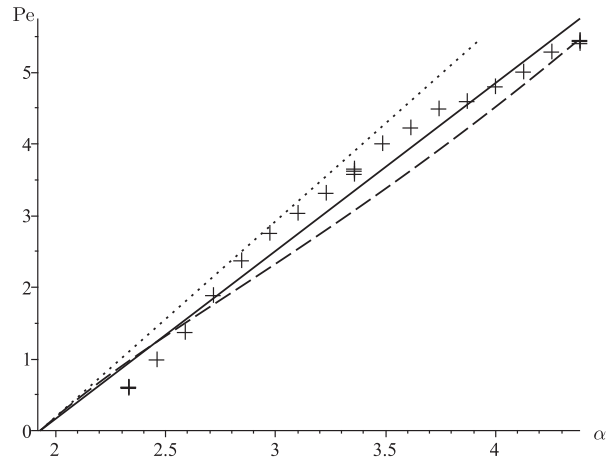

FIG. 11. Graph of solution using averaged conditions. Dashed curve: (3.20) (five terms). Dotted curve: (3.22). Crosses: PLA experimental data (with linear fit). Note the lack of curve-like behavior in the solutions.

7. Conclusions and further research

To optimize production using a 3D printing process, it is important to know the maximum rate at which the polymer construction material can be extruded. Given the maximum rated temperature for the hot end, there exists an upper bound on the velocity at which the polymer may be extruded. Beyond that velocity, the polymer has not been heated enough to become pliant enough to be extruded through the nozzle.

After making several physically realistic simplifying assumptions, we modeled the system by the heat equation in cylindrical coordinates. In the amorphous case, the problem may be solved by separation of variables; in the crystalline case it becomes a Stefan problem, which we solved using the quasistationary approximation.

The more subtle point is to determine what type of conditions need to be placed on the solution to match the calculated upper bound to experimental data. In particular, what must be true about the temperature or viscosity to guarantee that the polymer will remain pliant enough to extrude through the unheated nozzle?

We examined three possibilities. The pliancy of the polymer depends on it being above a certain temperature. Therefore, a reasonable possibility would be to require that the minimum exit temperature (along the axis) be above a certain threshold. However, as shown in Figs. 3, 6 and 9, using this condition led to curves in the α-Pe plane that did not match the experimental data.

The extrusion process fails when the insertion pump cannot provide enough pressure to force the polymer through the nozzle. Thus, another reasonable possibility would be to require that the pressure head be above a certain value. We showed that this condition is equivalent to the average viscosity in the polymer being above a certain value. By using some simplifying averaging assumptions, we established a bound on the velocity, which produced straight-line data. However, given the material constants of the various polymers, such a condition produced wildly different estimates of the velocity bound as compared to experimental data (see Figs. 4, 7 and 10).

Lastly, we note that the extrusion process must rely upon the polymer being reasonably pliant not only at the exit of the hot end, but throughout. Therefore, the final condition we tested was to require that the average temperature of the polymer in the heated region be above a certain temperature. In the amorphous case, this condition produced predictions that matched well with experimental results (see Figs. 5 and 11).

However, in the crystalline case, even this third condition did not produce reasonable results. Happily, we noted that if we treated a crystalline polymer such as PLA as if it underwent only the amorphous transition, the ensuing mathematical results would fit the experimental data. PLA is a slowly crystallizing polymer, and during its manufacture the fiber is quenched rapidly from the melt to produce amorphous material. So the feed material into the hot end is amorphous (as our results have shown) and one may suggest that the amorphous case should apply. However, a quenched crystalline polymer will crystallize when heated above T_g (but still below T_m) (Hiemenz & Lodge, 2007). The analysis provided here demonstrates that this effect is negligible.

Our results demonstrate that using the average temperature as a mathematical condition for the amorphous model produces an estimate for the velocity upper bound, which matches well with experimental data, no matter the type of polymer used.

The model in this manuscript contains several listed simplifications and assumptions. Relaxing them and considering more complicated models is an area for fruitful further research. For instance, given that the failure mode of the device is pressure buildup, we surmise that global properties in the hot end are crucial. Therefore, another condition to consider would be to maximize the volume of pliant polymer in the hot end—in other words, to maximize the medium shaded area in Fig. 1.

Obviously, improving the mathematical sophistication of the solution will be beneficial. In particular, the quasistationary assumption for crystalline polymers could be relaxed, with an eye to doing so in a way that would make the model for crystalline polymers more experimentally realistic.

Nomenclature

Variables and parameters

Units are listed in terms of length (L), mass (M), time (T) and temperature (θ). If a symbol appears both with and without tildes, the symbol with tildes has units, while the one without is dimensionless.

Equation numbers where a variable is first defined is listed, if appropriate.

a: parameter used in crystalline model (5.7).

c_{L}: latent heat of melting, units L^2/T^2 (4.2).

c_p: heat capacity of polymer, units $L^2/(T^2\theta)$ (2.1).

H: length of heater, units L (2.2).

I: integral used in viscosity calculation of crystalline model (5.6b).

k: thermal conductivity, units $ML/(T^3\theta)$ (2.1).

n: indexing variable (3.1b).

p: pressure (3.8).

Pe: Péclet number (2.3).

R: radius of cylinder.

$\tilde{r}$: radial coordinate, units L (2.1).

St: Stefan number (4.2).

$s(z)$: front between phases, units L (4.1).

$\tilde{T}(\tilde{r},\tilde{z})$: temperature, units θ (2.1).

$u(z)$: $[s(z)]^2$ (4.10a).

V: velocity in $\tilde{z}$-direction, units L/T (2.1).

v_z: velocity profile in z-direction (3.8).

y: dummy variable.

$\tilde{z}$: distance along the channel, units L (2.1).

α: dimensionless temperature at heater (2.4a).

β: coefficient in viscosity calculation (3.16).

ΔT: differential between transition and room temperature, units θ (2.2).

δ: small radius.

$\Theta(r,z)$: heat function used in amorphous case (3.1a).

μ: viscosity (3.7).

ρ: density of polymer, units M/L^3 (2.1).

Other Notation

g: as a subscript on T, used to indicate the temperature of the glass–rubber transition.

i: as a subscript on T, used to indicate the initial temperature (2.2).

m: as a subscript on T, used to indicate the melting temperature.

max: as a subscript, used to indicate the heater (2.1).

p: as a subscript on T, used to indicate temperature in the pliant region (2.4a).

r: as a subscript on T, used to indicate temperature in the rigid region (2.4b).

t: as a subscript, used to indicate the extrusion transition (3.4).

μ: as a subscript on T, used to indicate a characteristic temperature in the viscosity formula (3.7).

*: as a subscript on T, used to indicate the pliancy temperature (2.2).

$\langle\cdot\rangle$: used to indicate a cross-sectional average (3.9).

$\bar{\ }$: used to indicate an average over the whole device (3.11).

Acknowledgements

We thank the reviewers for their helpful comments which improved the manuscript. Many of the calculations herein were performed with the assistance of Maple.

Reference

Alexiades, V. & Solomon, A. D. (1992) *Mathematical Modeling of Melting and Freezing Processes*. Taylor & Francis.

Bird, R. B., Stewart, W. E. & Lightfoot, E. N. (1960) *Transport Phenomena*. New York: Wiley.

Carrier, G. F. & Pearson, C. E. (1988) *Partial Differential Equations: Theory and Technique*. New York: Academic Press.

Gibson, I., Rosen, D. W. & Stucker, B. (2009) *Additive Manufacturing Technologies: Rapid Prototyping to Direct Digital Manufacturing*, 1st edn. Springer Publishing Company Incorporated.

Hiemenz, P. & Lodge, T. (2007) *Polymer Chemistry*, 2nd edn. Taylor & Francis.

Lotero, F., Couenne, F., Maschke, B. & Sbarbaro, D. (2017) Distributed parameter bi-zone model with moving interface of an extrusion process and experimental validation. *Math. Comput. Model. Dyn. Syst.*, **23**, 504–522.

Mackay, M. E., Swain, Z. R., Banbury, C. R., Phan, D. D. & Edwards, D. A. (2017) The performance of the hot end in a plasticating 3D printer. *J. Rheol.*, **61**, 229–236.

Mu, Y., Zhao, G., Wu, X., Hang, L. & Chu, H. (2015) Continuous modeling and simulation of flow-swell-crystallization behaviors of viscoelastic polymer melts in the hollow profile extrusion process. *Appl. Math. Model.*, **39**, 1352–1368.

Pyda, M., Bopp, R. C., & Wunderlich, B. (2004) Heat capacity of poly(lactic acid). *J. Chem. Thermodyn.*, **36**, 731–742.

Sandoval Murillo, J. L. & Ganzenmueller, G. C. (2017) A convergence analysis of the affine particle-in-cell method and its application in the simulation of extrusion processes. *V International Conference on Particle-Based Methods - Fundamentals and Applications (Particles 2017)* (P. Wriggers, M. Bischoff, E. Onate, D. R. J. Owen & T. Zohdi eds). European Community on Computational Methods in Applied Sciences; International Association for Computational Mechanics, pp. 397–408.

Schoinochoritis, B., Chantzis, D. & Salonitis, K. (2017) Simulation of metallic powder bed additive manufacturing processes with the finite element method: a critical review. *Proc. Inst. Mech. Eng. B J. Eng. Manuf.*, **231**, 96–117.

Sneddon, I. N. (1960) On some infinite series involving the zeros of Bessel functions of the first kind. *Proceedings of the Glasgow Mathematical Association*, vol. **4**. Cambridge University Press, pp. 144–156.

Appendix

In Table A1 we list the parameters for the hot end. Some are from the experimental paper Mackay *et al.* (2017), while others come directly from measurements in the lab. As hypothesized, the aspect ratio of the cylinder is small $O(10^{-2})$.

TABLE A1 *General device parameters*

	Mackay *et al.* (2017)	Used
D (mm)	3.175	
H (mm)		30
T_i (°C)		20

In Table A2 we list the parameters for ABS. In the left column are experimental parameters; the values of the calculated parameters are listed at right. As expected, we are in the regime of relatively small Pe and α.

TABLE A2 *Parameters for ABS*

	Experimental Mackay *et al.* (2017)	Used	Calculated	
c_p [J/(kg·K)]	2100		Pe	0.219–3.26
k [W/(m·K)]		0.205	T_t	0.906
T_{max} (°C)	175–245		α	0.938–1.81
T_* (°C)	100		β	8.16
$\tilde{T}_t$ (°C)	169–174		ΔT (K)	80
$\tilde{T}_\mu$ (K)	10700			
V (mm/s)	0.23–3.44			
ρ (kg/m^3)		1100		

In Table A3 we list the parameters for PLA needed to use the crystalline model. As noted in the text, for this model we take only those experiments with high enough values of T_{max} that we think we may be in the melt regime, namely those with T_{max} sufficiently greater than T_m. Again we are in the regime of relatively small Pe and α.

TABLE A3 *Parameters for PLA (crystalline model: Section 5)*

	Experimental Mackay *et al.* (2017)	Pyda *et al.* (2004)	Calculated	
c_L (kJ/kg)		91	a	-9.37×10^{-2}
c_p [J/(kg·K)]	1700		Pe	0.551–5.08
k [W/(m·K)]	0.13		St	2.52
T_{max} (°C)	170–230		T_t	−0.283
$T_* = T_m$ (°C)	155		α	1.11×10^{-1}–5.56×10^{-1}
$\tilde{T}_t$ [°C]	138–143		β	7.90
$\tilde{T}_\mu$ (K)	12400		ΔT (K)	135
V (mm/s)	0.4–3.69			
ρ (kg/m^3)	1250			

TABLE A4 *Parameters for PLA (amorphous model: Section 6)*

	Experimental Mackay *et al.* (2017)	Calculated	
T_{max} (°C)	150–230	T_t	1.93
$T_* = T_g$ (°C)	59	α	2.33–4.38
		β	8.81
		ΔT (K)	39

In Table A4 we list the parameters for PLA needed to use the amorphous model. For this model, we use all the experiments, no matter their value of T_{max}.